Joint EPRI – 123HiMAT International Conference on
Advances in High Temperature Materials
October 21–24, 2019, Nagasaki, Japan
J. Shingledecker, M. Takeyama, editors
https://doi.org/10.31339/asm.cp.am-epri-2019p0441

Generation behavior of abnormally large grain in superalloy 718

Chuya Aoki
Yasugi Works, Engineering & Solutions Department, Hitachi Metals, LTD., 2107-2 Yasugi-cho, Yasugi, Shimane, 692-8601, Japan

Masayoshi Date, Tomonori Ueno, Takehiro Ohno
Metallurgical Research Laboratory, Hitachi Metals, LTD., 1240-2 Hashima, Yasugi, Shimane, 692-8601, Japan

Katsunari Oikawa
Department of Metallurgy Graduate School of Engineering, Tohoku University, Aoba-6-6-02, Aramaki, Aoba-ku, Sendai, Miyagi, 980-8579, Japan

ABSTRACT
The behavior of strain-induced abnormal grain growth (AGG) in superalloy 718 has been investigated using compression testing and subsequent heat treatment below the δ-phase solvus temperature of 980 °C. The nuclei of AGG grains were slightly newly recrystallized grains by a nucleation because small grains without dislocation was observed in the as-deformed microstructure. AGG was caused by the difference in intragranular misorientation (related to the stored strain energy in a grain) between dynamic recrystallized grains and deformed matrix. The initiation of AGG was retarded with decreasing plastic strain and produced microstructures consisted of larger grains having more complex morphology. It was observed that grain boundary migrated locally in the direction perpendicular to, or mainly in the direction parallel to the Σ3 {111} twin boundaries along with the formation of high-order twins. As a result of multiple twinning, AGG grains seemed to evolve with the growing directions changed.

KEYWORDS
718 superalloy, abnormal grain growth, recrystallization, twin, in-situ annealing

INTRODUCTION
Superalloy 718 is a nickel-based alloy widely used for applications in aircraft engines and power generation turbines. These technologies usually require alloys with a fine-grained microstructure to achieve high fatigue lifetimes. During the manufacture of superalloy 718, hot-working processes below the δ-phase solvus temperature (950–1010 °C) are used to control the microstructure. Particles of the δ phase inhibit the grain growth of the matrix after recrystallization, thus ensuring a fine-grained microstructure and good fatigue properties [1]. However, abnormal grain growth (AGG) often occurs, which coarsens the matrix grains. It was reported that low prior plastic strains caused AGG during heat treatment below the δ-phase solvus temperature [2-8], thereby decreasing the low cycle fatigue lifetimes [9]. The AGG phenomenon induced by low plastic strains has also been observed in other superalloys [10-12], electrical steel [13,14] and materials obtained by grain boundary engineering [15-17] to improve intergranular corrosion, termed twin related domains (TRDs) due to the formation of a heavily twinned microstructure [18,19]. Barr et al. [18] investigated the twinning mechanism in the coarsening process of TRDs regarding austenitic stainless steel 316L, and clarified that twin boundaries formed behind the

migrating grain boundary front which is parallel to the {111} planes. We demonstrated that the AGG of superalloy 718 was accompanied by an increase in the twin boundary ratio, but the correlation of the AGG process with the formation of twin boundaries was still unclear [7,8]. The present study has been undertaken with the aim of elucidating the detailed mechanisms of AGG generation and progress by careful observation of microstructures.

EXPERIMENTAL PROCEDURES

The superalloy 718 billet (Fe-54Ni-18Cr-3Mo-0.5Al-1Ti-5.4Nb-0.025C mass %) was forged into disks by upset forging and subsequent ring rolling at 980 °C (below the δ-phase solvus temperature). Coupons were cut from the ring-rolled material, such that the compression axis was parallel to the tangential direction. In this study, we used two types of double-cone specimens [10] that differ in size. A 14-mm-high specimen (specimen A) was machined from coupons that had been pre-heat-treated at 980 °C for 1 h, and then subjected to the compression test in a servo hydraulic facility equipped with an induction heating system. The initial microstructure pre-heat-treated at 980 °C was a fine-grained structure with grain size of ~12 μm, and the δ-phase particles, comprising ~5% of the area, were homogeneously distributed, as shown in our previous study [7,8]. After heating specimen A samples at 980 °C, they were deformed at 980 °C, with a 10 to 30% reduction in height at a constant displacement rate of 7 mm/s (nominal strain rate 0.5 s^{-1}), and subsequently annealed at 980 °C for 0 to 240 s. An 84-mm high specimen (specimen B) was machined from coupons without pre-heat treatment (because of later heating for hot compression), and then subjected to the compression test using a hydraulic facility equipped with resistance-heated forging dies. Specimen B samples were deformed upon heating at 980 °C for 1 h, exhibiting a 12% reduction in height at a constant displacement rate of 42 mm/s (nominal strain rate 0.5 s^{-1}) or 0.42 mm/s (nominal strain rate 0.005 s^{-1}), with upper and lower dies heated at about 980 °C, followed by water quenching. Solution heat treatment was subsequently carried out at 980 °C for 1 h.

The specimens were cut in half along the longitudinal axis after deformation and subsequent annealing and solution heat treatment, and were then polished to allow observation of the microstructures of the longitudinal sections. The microstructures of the deformed and annealed specimen A samples were observed using electron backscatter diffraction (EBSD; Digiview 4, EDAX). The EBSD scans were performed using a scanning electron microscope (SEM; ULTRA 55, Carl Zeiss AG Corporation) equipped with an EBSD detector. The microstructure of as-deformed specimen B samples was observed using transmission electron microscope (TEM; JEM-2100PLUS, JEOL), and EBSD (Hikari SUPER, EDAX) with in-situ annealing. The TEM examination was conducted at an accelerating voltage of 200 kV. The extracted samples for EBSD measurement with in-situ annealing were mechanically polished with colloidal silica to a mirror surface, and then annealed in an SEM (JSM-7001F, JEOL) chamber at 980 °C. The microstructure of specimen B samples after solution heat treatment was also observed using EBSD (Digiview 4, EDAX). To evaluate the microstructures, the grain orientation spread (GOS), which is defined as the average of the intragranular misorientation of each measurement point and the average orientation of all the measurement points in the grain, and crystallographic orientations were evaluated using the TSL OIM analytical software 7 (TSL Solutions, 2015).

RESULTS

Behavior of microstructural evolution

Detailed microstructural observation of the deformed specimen A during annealing was carried out to understand the microstructural evolution behavior. Fig. 1 shows GOS maps overlapped with maps of both the grain boundaries and the Σ3 twin boundaries with respect to different plastic strains, and annealing time. It is observed that the microstructural evolution during annealing is accompanied by a decrease in GOS, which is related to stored strain energy in grains. In addition, the decrease in GOS slows down with decreasing plastic strain because a high-GOS region remains in the low-strain sample after 60 s (Fig. 1a). Recrystallized grains with low GOS are observed at plastic strains of 0.26 and 0.58 in the as-deformed sample (annealing time 0 s), as shown in Figs. 1c and 1d. It is noticed that small grains with low GOS are observed slightly, even at low plastic strains of 0.1 and 0.07, as indicated by the black arrows in Figs. 1a and 1b. Such low plastic strains might be the nuclei of the AGG structure, as mentioned in our previous study [8].

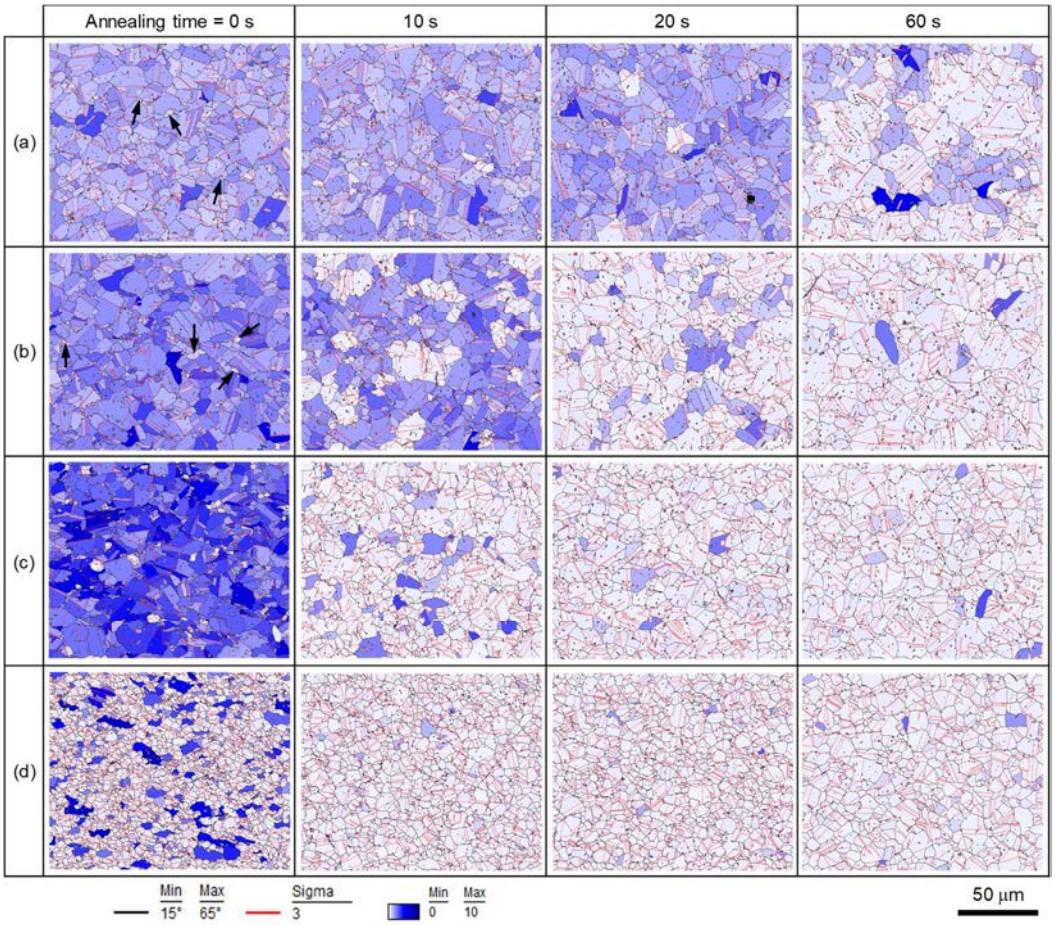

Figure 1: GOS maps overlapped by grain boundaries and twin boundaries for the microstructures of specimen A deformed at 980 °C at a displacement rate of 7 mm/s and subsequently annealed at 980 °C for 0, 10, 20 and 60 s. (a) ε = 0.07, (b) ε = 0.1, (c) ε = 0.26, (d) ε = 0.58

Fig. 2 shows the TEM micrographs of the microstructure at the position corresponding to a plastic strain of 0.1 for specimen B sample deformed at 980 °C at a displacement rate of 42 mm/s, indicating that the low dislocation-free grains shown in Figs. 2a-c were created in the deformed matrix with high-density dislocation, shown in Fig. 2d. These results suggest that AGG is a primary recrystallization phenomenon that is generated by a stored strain energy, as mentioned by Agnoli et al. [5] for Inconel 718. Moreover, Fig. 2 demonstrates that the nuclei of AGG grains appear to be the nucleation sites of newly recrystallized grains.

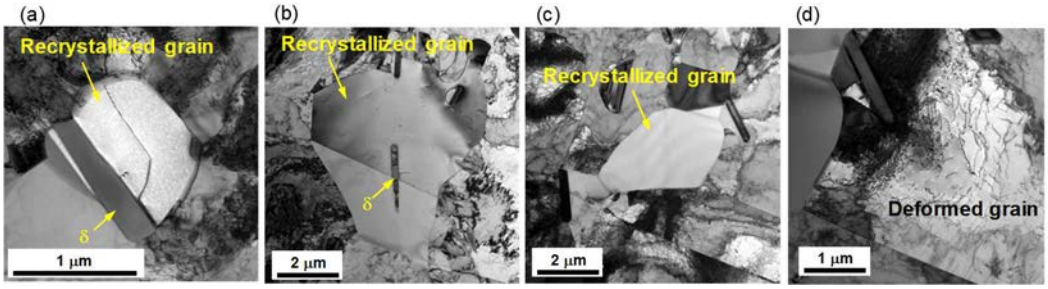

Figure 2: TEM micrographs of the microstructure oriented to [011] at the position of plastic strain 0.1 for specimen B deformed at 980 °C at a displacement rate of 42 mm/s. (a) (b) (c) Recrystallized grain. (d) Deformed grain

Behavior of twin boundary in AGG grain

The correlation between crystal orientation and morphology of the recrystallized grains of specimen B was investigated. Fig. 3 is the macrograph showing the evaluated position of the solution heat-treated specimen B after deformation at 980 °C to 12% reduction and a displacement rate of 0.42 mm/s.

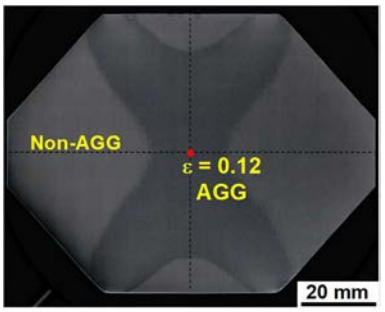

Figure 3: The macrograph of cross-section showing EBSD measurement area for the solution heat treated specimen B after deformation at 980 °C to 12% reduction and a displacement rate of 0.42 mm/s.

Figs. 4a and 4b exhibit the results of EBSD measurement for the AGG grains having higher-order twins, corresponding to a plastic strain of 0.12 for solution heat-treated specimen B after deformation at 980 °C and a displacement rate of 0.42 mm/s. The parent grain G1 has primary (T1), secondary (T2 and T3) and tertiary (T4) twins in the AGG grain of Fig. 4a. Fig. 4b shows the {111} and {110} pole figures (PFs) for this parent grain and each twin. Based on the inverse pole figure (IPF) map and the {111} PFs, the formation

of the twins T3 and T4 produces a change in the growing direction perpendicular to the Σ3 {111} twin boundaries (B ⇒ C or B ⇒ c). In addition, the twin T2 that originates from the twin T1 tries to surround the neighboring grain by growing in the direction a, as seen in the circle area in Fig. 4a. From observation of the AGG grain, it appears that the AGG grain develops a complex morphology accompanied by the formation of twins and growing in the direction perpendicular to the Σ3 {111} twin boundaries, which is similar to the results presented by Barr et al. [18]. However, it is observed that grain boundary migrates mainly in the direction parallel to the Σ3 {111} twin boundaries. In order to identify the direction parallel to the Σ3 {111} twin boundaries, we focused on the rectangle area in Fig. 4a, which consists of the parent grain G1, the primary twin T1 and the secondary twin T2. They have only one common ⟨110⟩ axis (direction D and d), as shown in the {110} PFs of Fig. 4b. Fig. 4c illustrates the regular octahedron arrangement surrounded by the {111} of the parent grain, primary twin and secondary twin. It is supposed that the parent grain, the primary twin and secondary twin have different crystallographic orientations, but easily grow in the common ⟨110⟩ direction because the arrangement of atoms is consistent.

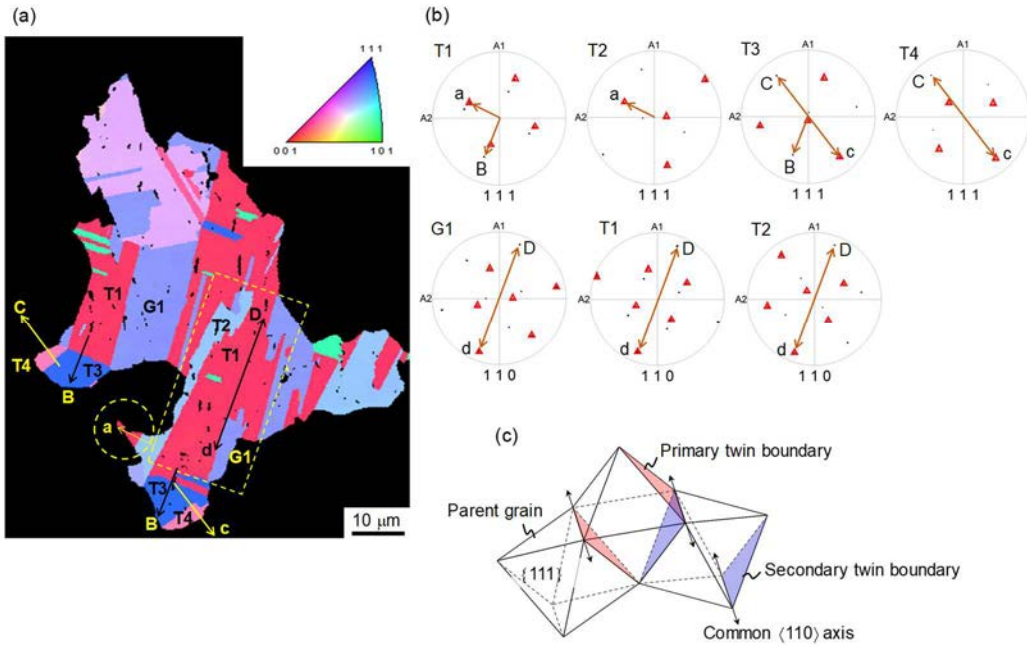

Figure 4: EBSD results of the recrystallized grain at a plastic strain of 0.12 for the solution heat-treated specimen B after deformation. (a) IPF map. (b) {111} and {110} PFs for the parent grain (G1) and the individual twins (T1-T4) in the recrystallized grain. The poles in triangle symbols on the {111} or {110} PFs show the directions normal to the {111} and {110} in the negative hemisphere. (c) Illustration of regular octahedron arrangement surrounded by the {111} of the parent grain, primary twin and secondary twin.

The growth in the direction parallel to the Σ3 {111} twin boundaries was also confirmed by in-situ annealing. Figs. 5a and 5b show the EBSD results measured during in-situ annealing of the cut-out sample corresponding to a plastic strain of 0.12 for specimen B

deformed at 980 °C and a displacement rate of 0.42 mm/s. The parent grain G2, and the primary twins T5 and T6 were observed to grow in the common ⟨110⟩ direction (direction E and e) at 980 °C for 35 min. Fig. 5c illustrates the regular octahedron arrangement surrounded by the {111} of the parent grain and the two different primary twins, showing that only one common ⟨110⟩ direction exists. Based on the observation that grain boundary migration is not only perpendicular to twin boundaries but also parallel to twin boundaries, the formation of twins is likely to be based on the growth accident model of Mahajan *et al.* [20] (grain boundary migration is associated with stacking of atoms on {111} steps from shrinking grains).

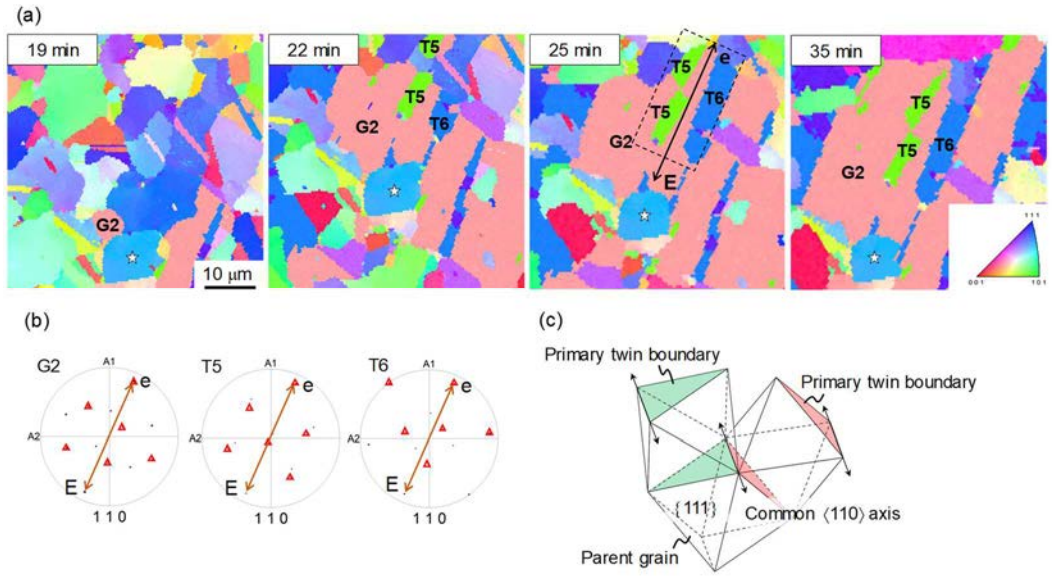

Figure 5: EBSD results measured during in-situ annealing of the sample extracted at a plastic strain of 0.12 for specimen B deformed at 980 °C. (a) IPF maps at the state of 19, 22, 25 and 35 min of annealing at 980 °C, respectively. (b) {110} PFs for the parent grain (G2) and the individual twins (T5 and T6) in the recrystallized grain. The poles in triangle symbols of the {111} or {110} PFs show the directions normal to the {111} or {110} in the negative hemisphere. (c) Illustration of regular octahedron arrangement surrounded by the {111} of the parent grain and two different primary twins.

CONCLUSIONS

The initiation and progress behavior of AGG grains of superalloy 718 with initial grain size of about 12 μm in diameter was investigated through hot-working and subsequent process. The results are summarized as follows.

1. A very small number of recrystallized grains coarsened during heat treatment, inducing an AGG microstructure. AGG was formed through the recrystallization phenomenon.
2. AGG microstructures consisting of larger grains of more complex morphology developed when exposed to a decreased plastic strain. AGG grains grew predominantly perpendicular to the Σ3 twin boundaries in the ⟨111⟩ direction and parallel to the Σ3 twin boundaries in the ⟨110⟩ direction through multiple twinning.

ACKNOWLEDGMENTS
This work was supported by the Council for Science, Technology and Innovation (CSTI), Cross-ministerial Strategic Innovation Promotion Program (SIP), “Structural Materials for Innovation” (Funding agency: JST)

REFERENCES
[1] B. Pieraggi, and J.F. Uginet: Superalloys 718, 625, 706 and Various Derivatives, ed. E. A. Loria, (Warrendale, PA: TMS, 1994), pp. 535-544.
[2] J.F. Uginet, and B. Pieraggi: Superalloys 718, 625, 706 and Various Derivatives, ed. E. A. Loria, (Warrendale, PA: TMS, 1997), pp. 343-352.
[3] R. Watson, M. Preuss, J. Quinta de Fonseca, T. Witulski, and G. Terlinde: Superalloys 718, 625, 706 and Various Derivatives, ed. E. A. Loria, (Warrendale, PA: TMS, 2014), pp. 873-884.
[4] A. Agnoli, M. Bernacki, R. Logé, J.M. Franchet, J. Laigo, and N. Bozzolo: Superalloys 2012, eds. E. S. Huron et al., (Warrendale, PA: TMS, 2012), pp. 73-82.
[5] A. Agnoli, M. Bernacki, R. Logé, J.M. Franchet, J. Laigo, and N. Bozzolo: Metallurgical and Materials Transaction A, 2015, vol. 46A, pp. 4405-4421.
[6] R. Schwant, S. Thamboo, L. Yang, and M. Morra: Superalloys 718, 625, 706 and Various Derivatives, ed. E. A. Loria, (Warrendale, PA: TMS, 2005), pp. 15-24.
[7] C. Aoki, T. Ueno, and T. Ohno: Superalloys 2016, eds. M. Hardy et al., (Warrendale, PA: TMS, 2016), pp. 609-617.
[8] C. Aoki, T. Ueno, T. Ohno, and K. Oikawa: Journal of Materials Processing Technology, 2019, vol. 267, pp. 26-33.
[9] B. Flageolet, O. Yousfi, Y. Dahan, P. Villechaise, and J. Cormier: Superalloys 718, 625, 706 and Various Derivatives, ed. E. A. Loria, (Warrendale, PA: TMS, 2010), pp. 595-606.
[10] E. Huron, S. Srivatsa, and E. Raymond: Superalloys 2000, eds. T. M. Pollock et al., (Warrendale, PA: TMS, 2000), pp. 49-58.
[11] V.M. Miller, A.E. Johnson, C.J. Torbet, and T.M. Pollock: Metallurgical and Materials Transactions A, 2016, vol. 47A, pp. 1566-1574.
[12] I.M.D. Parr, T.J. Jackson, M.C. Hardy, D.J. Child, C. Argyrakis, K. Severs, V. Saraf, and J.M. Stumpf: Superalloys 2016, eds. M. Hardy et al., (Warrendale, PA: TMS, 2016), pp. 447-456.
[13] T.A. Bennett, P.N. Kalu, and A.D. Rollett: Scripta Materialia, 2007, vol. 57, pp. 41-44.
[14] T.A. Bennett, P.N. Kalu, and A.D. Rollett: Microscopy and Microanalysis, 2011, vol. 17, pp. 362-367.
[15] T. Watanabe, and S. Tsurekawa: Acta Materialia, 1999, vol. 47, pp. 4171-4185.
[16] C.A. Schuh, M. Kumar, and W.E. King: Acta Materialia, 2003, vol. 51, pp. 687-700.
[17] V. Randle: Acta Materialia, 2004, vol. 52, pp. 4067-4081.
[18] C.M. Barr, A.C. Leff, R.W. Demott, R.D. Doherty, and M.L. Taheri: Acta Materialia, 2018, vol. 144, pp. 281-291.
[19] T.S. Prithiv, P. Bhuyan, S.K. Pradhan, V.S. Sarma, and S. Mandal: Acta Materialia, 2018, vol. 146, pp. 187-201.
[20] S. Mahajan, C.S. Pande, M.A. Imam, and B.B. Rath: Acta Materialia, 1997, vol. 45, pp. 2633-2638.